Published in final edited form as:

Curr Biol. 2019 July 22; 29(14): 2259–2269.e4. doi:10.1016/j.cub.2019.05.075.

Kinesin-5 promotes microtubule nucleation and assembly by stabilizing a lattice-competent conformation of tubulin

Geng-Yuan Chen[1,4], **Joseph M. Cleary**[1], **Ana B. Asenjo**[2], **Yalei Chen**[3], **Jacob A. Mascaro**[1,5], **David F. J. Arginteanu**[1], **Hernando Sosa**[2], **William O. Hancock**[1,6,*]

[1]Department of Biomedical Engineering and Bioengineering, Pennsylvania State University, University Park, PA 16802, USA

[2]Department of Physiology and Biophysics, Albert Einstein College of Medicine, Bronx, NY 10461, USA

[3]Center for Bioinformatics, Department of Public Health Sciences, Henry Ford Health System, Detroit, MI, USA

[4]Present address: Department of Biology, University of Pennsylvania, Philadelphia, PA 19104, USA

[5]Present address: School of Medicine, University of West Virginia, Morgantown, WV 26506, USA

[6]Lead Contact

Summary:

Besides sliding apart antiparallel microtubules during spindle elongation, the mitotic kinesin-5, Eg5 promotes microtubule polymerization, emphasizing its importance in mitotic spindle length control. Here, we characterize the Eg5 microtubule polymerase mechanism by assessing motor-induced changes in the longitudinal and lateral tubulin-tubulin bonds that form the microtubule lattice. Isolated Eg5 motor domains promote microtubule nucleation, growth and stability; thus, crosslinking tubulin by pairs of motor heads is not necessary for polymerase activity. Eg5 binds preferentially to microtubules over free tubulin, which contrasts with microtubule-depolymerizing kinesins that preferentially bind free tubulin over microtubules. Colchicine-like inhibitors that stabilize the bent conformation of tubulin allosterically inhibit Eg5 binding, consistent with a model in which Eg5 induces a curved-to-straight transition in tubulin. Domain swap experiments establish that the family-specific Loop11-helix 4 junction, which resides near the nucleotide-

*Lead Contact and Correspondence should be addressed to: William O. Hancock, Department of Biomedical Engineering, 430 CBEB, Pennsylvania State University, University Park, PA, 16802, USA, Phone: (814) 863-0492, wohbio@engr.psu.edu.

Author Contributions

G.-Y.C., Y.C., and W.O.H. initiated the project. G.-Y.C. and W.O.H. designed experiments, developed models, and prepared the manuscript. G.-Y.C., J.M.C. and D.F.J.A. prepared reagents and carried out experiments. G.-Y.C and J.M. carried out simulations and pilot studies of microtubule shrinkage. G.-Y.C. and A.B.A. generated samples for negative staining EM. A.B.A. and H.S. acquired and analyzed EM images.

Declaration of Interests

The authors declare no competing interests.

sensing Switch-II domain, is necessary and sufficient for the polymerase activity of Eg5. Thus, we propose a microtubule polymerase mechanism in which Eg5 at the plus-end promotes a curved-to-straight transition in tubulin that enhances lateral bond formation and thereby promotes microtubule growth and stability. One implication is that regulation of Eg5 motile properties by regulatory proteins or small molecule inhibitors could also have effects on intracellular microtubule dynamics.

eTOC blurb:

Mitotic kinesin-5 (Eg5) motors promote microtubule polymerization through an unknown mechanism. Chen *et al.* propose a model in which Eg5 binding to tubulin promotes a curved-to-straight transition that drives microtubule assembly. During mitosis, this polymerase activity may enhance spindle formation and stability, and drive poleward flux.

Keywords

Kinesin; Eg5; microtubule; microtubule dynamics; tubulin wedge inhibitors; microtubule-associated proteins; coupled-equilibria

Introduction

Faithful segregation of genetic material and interior cellular contents to daughter cells requires tight control of mitotic spindle size and architecture. Stochastic switching between microtubule growth and shrinkage enables assembly and dynamic remodeling of the mitotic spindle, and these microtubule dynamics are mediated by dozens of regulatory proteins. Understanding the spatiotemporal regulation of microtubule dynamics during mitosis is essential for uncovering mechanisms that cells employ to ensure proper chromosome segregation.

Tubulin subunits are held in the microtubule lattice by both longitudinal tubulin-tubulin contacts that stabilize protofilaments, and lateral contacts that join adjacent protofilaments. Incorporation of tubulin into the lattice is determined by the tubulin nucleotide state, with the textbook explanation being that GTP-tubulin adopts a straight conformation that readily incorporates into the lattice, whereas GDP-tubulin adopts a curved conformation. However, more recent work has shown that soluble tubulin with either GTP- or GDP-bound adopt a curved conformation [1, 2], suggesting that growth at the microtubule plus-end requires the incoming tubulin to undergo a curved-to-straight transition before being incorporated into the lattice. Consistent with this, images of growing microtubule plus-ends often show curled protofilaments in which longitudinal contacts have formed, but lateral contacts that require the curved-to-straight transition have not yet formed [3]. One prediction of this model is that biasing the curved-to-straight transition of tubulin by mutagenesis [4, 5], small-molecule inhibitors [6, 7], or other means should affect lateral bond stability and generally promote microtubule polymerization.

Kinesin motor proteins have been shown to alter microtubule dynamics and stability, with the best-studied examples being the microtubule-depolymerizing kinesin-8s and kinesin-13s

[8–10]. There is both structural and biochemical evidence that these depolymerases preferentially bind to free tubulin and stabilize the curved conformation that is incompatible with lateral tubulin-tubulin bond formation [11–13]. There is also evidence that other kinesins, such as the mitotic kinesin-7 CENP-E, accumulate at microtubule plus-ends and enhance microtubule stability in vivo [14]; kinesin-1 has also been shown to stabilize microtubules against depolymerization in vitro [15, 16]. Interestingly, binding of kinesin-1 to microtubules was also shown to expand the lattice of GDP microtubules to match that of stable GMPCPP microtubules, providing a possible clue to the stabilization mechanism [15, 17]. However, the underlying mechanisms of microtubule stabilization by kinesins and whether these mechanisms differ across kinesin families remain unclear.

Tetrameric kinesin-5 is best known for sliding antiparallel microtubules apart during spindle formation, but in addition to its mechanical activities, there is evidence that kinesin-5 motors also alter microtubule dynamics. Based on knockouts of Cin8 or Kip1 in budding yeast, Gardner and colleagues argued that yeast kinesin-5 motors act as microtubule depolymerases during anaphase [18]. However, other studies in budding yeast, and work in fission yeast found no evidence of fungal kinesin-5 depolymerase activity [19, 20]. For vertebrate kinesin-5, a dimeric construct of *Xenopus* Eg5 was shown to accumulate at microtubule plus-ends, enhance the microtubule growth rate and decrease the microtubule catastrophe frequency *in vitro* [21]; this microtubule polymerase activity was attributed to the ability of the two heads to “staple” together consecutive tubulin in a protofilament [22]. The apparent discrepancy between the *in vivo* yeast results and the *in vitro* vertebrate results remains unresolved.

In this study, we reveal the mechanism of the microtubule polymerase activity of vertebrate Eg5. Contrary to the expectation that the two heads of Eg5 “staple” together adjacent tubulin dimers, we find that monomeric Eg5 motor domains strongly promote microtubule nucleation, increase the microtubule growth rate, and stabilize the microtubule lattice against depolymerization. Quantitative assays show that Eg5 monomers preferentially bind to straight rather than curved tubulin, consistent with the mechanism being a complement to the tubulin curvature-sensing mechanism proposed for the kinesin-8 and kinesin-13 microtubule depolymerases. We find that the Loop11-helix 4 junction in Eg5 confers polymerase activity, and that swapping this structural element into kinesin-1 converts this transport motor into a polymerase. Taken together, our results illustrate that Eg5 drives a curved-to-straight transition in tubulin at the plus-end of a growing microtubule, which strengthens lateral tubulin-tubulin contacts and promotes microtubule assembly. This microtubule polymerase activity may play an important role in the ability of kinesin-5 to control spindle size and architecture in mitotic cells.

Results

Eg5 motors enhance microtubule plus-tip stability

To better understand the Eg5 microtubule polymerase mechanism, we visualized microtubules grown in the presence and absence of dimeric Eg5 using both total-internal reflective fluorescence (TIRF) microscopy and negative-stain electron microscopy (EM). When microtubules were polymerized from unlabeled tubulin in the presence of GFP-

labeled Eg5 dimers [21], motors were observed streaming along the microtubules and 20% of growing plus-ends (N = 16 out of 83 microtubules) had curved tapers that were observable by TIRF microscopy (Figure 1A). These plus-end curls had diameters of ~1 μm, much larger than "ram's horn" structures observed on depolymerizing microtubules, and many of the curved protofilament bundles subsequently straightened and were incorporated into the microtubule lattice (Video S1 and S2). In control experiments with kinesin-1, no plus-end curls were observed (N = 101 microtubules; not shown). When microtubules were examined in greater detail with negative-stain EM, sheets and ribbons consisting of bundles of protofilaments were observed at many microtubule ends, where both the frequency and length of the sheets were enhanced in the presence of Eg5 (Figure 1B–D and S1). Together, these results suggest that Eg5 motors stabilize microtubule plus-tip tapers.

Eg5 motors promote microtubule nucleation

Based on its stabilization of protofilaments at growing microtubule plus-ends, we hypothesized that Eg5 may also enhance microtubule nucleation [23]. To test this hypothesis, we polymerized microtubules starting from different free tubulin concentrations, immobilized the polymers on the surface of a coverslip, and counted the microtubules directly [24]. We found that at all tubulin concentrations, Eg5 motors increased the number of nucleated microtubules relative to control (Figure 1E–G). We also measured growth from short GMPCPP microtubule seeds [25] and found that Eg5 increased the fraction seeds that supported new growth across a range of tubulin concentrations (Figure S1). Thus, Eg5 lowers the critical concentration for microtubule nucleation. As an alternate method to assess nucleation, we carried out tubulin turbidity measurements to quantify the time-dependent increase in polymer mass, indicative of microtubule nucleation and growth (Figure 1H). In the absence of Eg5, the turbidity trace contains an initial lag (the nucleation phase), followed by a rising signal (the elongation phase) that eventually reaches a plateau. Addition of a physiologically relevant concentration of Eg5 in the reaction (130 nM) eliminated the lag phase (Figure 1H), indicative of a microtubule nucleator. Additionally, the steady-state turbidity signals at 60 minutes increased in the presence of Eg5 (Figure 1I), consistent with Eg5 promoting microtubule growth. Thus, Eg5 is both a *de novo* and a template-based microtubule nucleation promoter.

Monomeric Eg5 is sufficient to promote microtubule assembly

Because of its dimeric structure, we hypothesized that Eg5 promotes microtubule stabilization and nucleation by "stapling" consecutive tubulin on a given protofilament into the lattice. To test whether this crosslinking is necessary for Eg5 polymerase activity, we deleted the coiled-coil region to generate a monomeric Eg5 construct, $Eg5_M$ [22, 26], and used Interference Reflection Microscopy [49, 50] to quantify the microtubule growth rate in the presence of monomeric or dimeric Eg5 (Figure 2A–C). In the first experiment, we maintained a constant 7.5 μM tubulin concentration and varied motor concentrations at 25Ό. Dimeric Eg5 motors more than doubled the microtubule growth rate at this tubulin concentration, with half-maximal activity achieved at an EC_{50} 9 ± 1 nM (mean ± SE of fit; Figure 2D). This EC_{50} is considerably tighter than the motor's microtubule affinity of ~100 nM [22], likely due to concentration of motors at the plus-end (see Figure S1F–H). Surprisingly, monomeric $Eg5_M$ at high concentrations also promoted microtubule assembly,

with an EC_{50} of 84 ± 10 nM, establishing that stapling of adjacent tubulin by dimeric motors is not necessary for the Eg5 polymerase activity. We also found that, like Eg5 dimer, $Eg5_M$ shortened the lag time in the turbidity assay and enhanced microtubule numbers (Figure S2).

To further explore effects of Eg5 on microtubule dynamics, we grew microtubules at varying tubulin concentrations in the presence and absence of saturating concentrations of motors (Figure 2E). Growth velocities are traditionally fit to a line, where the slope and y-intercept correspond to the tubulin on- and off-rate constants, respectively, and the x-intercept is the critical concentration for elongation. Under control conditions at 25°C, t he critical concentration for growth was 3.6 ± 0.8 μM tubulin, and in the presence of dimeric Eg5, the critical concentration dropped to near zero (−0.1 ± 0.5 μM; mean ± SE of fit), demonstrating that motor binding strongly drives microtubule growth. In the presence of dimeric Eg5, the apparent tubulin on-rate constant of 1.6 ± 0.1 $\mu M^{-1}s^{-1}$ was increased to 2.2 ± 0.3 $\mu M^{-1}s^{-1}$ and the apparent tubulin off-rate slowed from 5.6 ± 1.2 s^{-1} to near zero (−0.3 ± 1.1 s^{-1}; all mean ± SE of fit). Hence, the reduction in critical concentration by dimeric Eg5 results from a slight increase in the apparent tubulin on-rate and a strong slowing of the tubulin off-rate. Eg5 monomers also reduced the critical concentration from 3.6 μM to 2.7 ± 1.1 μM tubulin, which was achieved by an increase in the on-rate from 1.6 to 2.2 ± 0.2 $\mu M^{-1}s^{-1}$ and a decrease in the tubulin off-rate from 5.6 to 4.2 s^{-1}. To test for monomer localization, we imaged Eg5M-GFP on taxol-stabilized microtubules and found no evidence for preferential plus end-binding or accumulation (Figure S2E). The fact that monomeric Eg5 required higher concentrations and resulted in a smaller smaller shift in critical concentration than the dimer is not surprising, as the dimer is able to processively walk to and concentrate at the plus-end to efficiently stabilize incoming tubulin, whereas the monomer must bind from solution to newly added tubulin at the plus-end to exert it stabilizing effects.

We next carried out microtubule shrinkage assays to assess whether Eg5 binding to the microtubule lattice enhances lattice stability. Microtubules were grown from immobilized seeds, the free tubulin was washed out to induce catastrophe, and the depolymerization rate measured in the absence and presence of motors (Figure 2F). Under control conditions, the shrinkage rate was 149 ± 7 nm/s, demonstrating that GDP-tubulin in the microtubule lattice rapidly dissociates from protofilament ends. In the presence of saturating concentrations of dimeric or monomeric Eg5 motors and ATP, the microtubule shrinkage rate slowed nearly 4-fold to 40 ± 2 nm/s and 30 ± 2 nm/s for Eg5 and $Eg5_M$, respectively. Thus, monomeric Eg5 motor domains bound to the lattice strongly enhance microtubule stability. To further investigate lattice stabilization by Eg5 monomer, we repeated the microtubule shrinkage assay in $Eg5_M$ under varying nucleotide conditions. In ADP, which induces a weak-binding state, the shrinkage rate was only 2-fold slower than control (80 ± 4 nm/s; titration curve in Figure S2D). In contrast, AMPPNP, no nucleotide (apo), or the Eg5 inhibitor BRD9876, all of which induce strongly-bound states of the motor [27], had “taxane-like” effects, generating super-stable microtubules (AMPPNP: 0.5 ± 0.05 nm/s; Apo: 4.7 ±0.18 nm/s; BRD: 0.2 ± 0.07 nm/s; Figure 2F). Hence, Eg5 motor domains bound to the lattice trap tubulin in the polymer form and reduce tubulin dissociation rates, and the degree of lattice stabilization scales with the strength of motor binding to the lattice.

Eg5 promotes tubulin assembly by preferentially binding to tubulin polymer

For microtubule-depolymerizing kinesins in the kinesin-8 and kinesin-13 families, the depolymerization mechanism can be explained by a thermodynamic cycle consisting of two linked equilibria – motor binding and microtubule assembly. In this formalism, the depolymerase activity can be explained as follows: motors bind more tightly to curved tubulin than to the microtubule lattice and thus motors shift tubulin toward the depolymerized state [11, 13]. By analogy, we propose a complementary mechanism for the Eg5 polymerase activity – Eg5 motors bind more tightly to microtubule polymer than to free tubulin, and thereby drive the system toward the polymerized state. In Figure 2H, we present a thermodynamic scheme describing motor binding and microtubule polymerization. Motor binding affinities to free tubulin and to the microtubule lattice are described by equilibrium constants K_{M1} and K_{M2}, respectively. Microtubule polymerization from free tubulin is described by equilibrium constants K_{D1} and K_{D2}, corresponding to the critical concentration for microtubule growth in the absence and presence of Eg5, respectively. If these linked equilibria are treated as a thermodynamic cycle, then it follows that:

$$K_{M1}K_{D2} = K_{D1}K_{M2}.$$

We carried out ATPase assays and used the K_M as a proxy for the equilibrium constant for Eg5 binding to tubulin (K_{M1}) and microtubules (K_{M2}). Monomeric Eg5 was employed here to avoid any complications from processivity of the dimer. From Figure 2G, K_{M1} = 9.9 ± 1.2 μM for the $Eg5_M$ tubulin-stimulated ATPase and K_{M2} = 0.6 ± 0.03 μM for the microtubule-stimulated ATPase. The K_{D1} value, corresponding to the critical concentration for growth under control conditions (Figure 2E) was K_{D1} = 3.6 μM. For dimeric Eg5, which could concentrate at the microtubule plus-end and thus exert is full influence, the critical concentration for growth was near zero (Figure 2E). If we estimate this K_{D2} to be 0.2 μM, then the products K_{M1} K_{D2} (9.9 μM * 0.2 μM) and K_{D1} K_{M2} (3.6 μM * 0.6 μM) agree. To summarize, preferential binding of Eg5 to microtubules over free tubulin (i.e. $K_{M2} < K_{M1}$) enhances assembly of tubulin into the polymer state in the presence of Eg5 (i.e. $K_{D2} < K_{D1}$). We next set out to understand the structural basis for the Eg5 microtubule polymerase mechanism.

Eg5-binding causes a structural change in tubulin that promotes polymerization

In the microtubule lattice, tubulin heterodimers adopt a straight conformation stabilized by both lateral and longitudinal interactions with neighboring subunits, whereas tubulin in solution adopts a curved conformation incompatible with lateral contacts [1, 2, 28]. Thus, compounds that promote or stabilize the curved to straight transition generally promote polymerization, whereas compounds that stabilize the curved conformation inhibit polymerization [29]. An example of the latter class of compounds are “intra-dimeric wedge inhibitors” such as colchicine derivatives and nocodazole that bind at the interface between α- and β-tubulin and are thought to freeze tubulin in the kinked conformation, which traps tubulins in the soluble state [6, 30].

Because monomeric Eg5 cannot directly crosslink adjacent tubulin-tubulin dimers, an alternate explanation is that Eg5 works allosterically by stabilizing the straight conformation of tubulin, which promotes lateral tubulin-tubulin interactions and thereby enhances microtubule growth. Structurally, the Eg5 binding site on the outer face of tubulin is located at the intradimeric junction between α- and β-tubulin, opposite to wedge inhibitor binding sites on the inner face of tubulin (Figure 3A). Based on this structural arrangement and the effects of different nucleotides on microtubule stabilization (Figure 2F), we propose that Eg5 binds free tubulin initially in a weakly-bound state, and upon tubulin binding, the motor releases its nucleotide and enters a strongly-bound state that stabilizes tubulin in a straight conformation that promotes microtubule assembly (Figure 3B). This model predicts that intradimeric wedge inhibitors like colchicine and nocodazole that stabilize the bent conformation of tubulin will antagonize Eg5 binding to tubulin and inhibit tubulin-stimulated nucleotide release and ATP turnover.

To test whether Eg5 binding induces a structural transition in tubulin, we first measured the binding affinity of the colchicine derivative demecolcine to tubulin in the presence or absence of motors (Figure 3C). We chose demecolcine because it binds tubulin with fast kinetics and it quenches tubulin intrinsic fluorescence, providing a convenient optical readout of drug binding [31]. Demecolcine binds to free tubulin with a K_D of 17 ± 1.3 μM, and in the presence of the microtubule depolymerizing kinesin-8, KLP67A, the drug binding affinity was unaffected, consistent with drug and motor having distinct binding sites (Figure 3D, S3A). In contrast, in the presence of $Eg5_M$ the K_D of demecolcine binding rose to 40 ± 1.6 μM, consistent with binding of Eg5 allosterically inhibiting drug binding (Figure 3C, D). Next, we measured the binding kinetics of colchicine to tubulin (Figure 3E). Previous work showed that the fluorescence signal consists of two phases, corresponding to an initial encounter, followed by a tubulin conformational change [32]. In the absence of Eg5, colchicine binding to tubulin was biexponential with a fast phase of 0.169 ± 0.004 s^{-1} and a slow phase of 0.048 ± 0.001 s^{-1} having equal amplitudes (Figure 3E). In the presence of Eg5, the amplitude of the fast phase dropped to ~3% of total, and the rate of the slow phase decreased fivefold to 0.0085 ± 0.0006 s^{-1}. This result supports a model in which Eg5 binding straightens tubulin, closes the binding pocket of the wedge inhibitor, and generates a species that favors microtubule polymerization.

Blocking the tubulin curved-to-straight transition slows the Eg5 nucleotide cycle

Because binding of Eg5 to tubulin diminishes the binding of tubulin wedge inhibitors, the converse should be true – tubulin wedge inhibitors should allosterically inhibit Eg5 binding to tubulin. Specifically, if Eg5-induced straightening of tubulin is coupled to the motor's nucleotide hydrolysis cycle, then wedge inhibitors that stabilize the bent conformation of tubulin should diminish Eg5 nucleotide release and ATP turnover. To measure motor-tubulin binding kinetics, we pre-incubated $Eg5_M$ with the fluorescent nucleotide mantADP, and flushed this species against varying concentrations of drug-bound tubulin plus unlabeled ADP. This experiment measures the kinetics of transitioning from State 1 to State 3 in Figure 3B. As a control, we first tested the interdimeric wedge inhibitor maytansinoid DM1, which is thought to bind between tubulin dimers and inhibit polymerization by blocking longitudinal interactions rather than altering tubulin curvature. Control and maytansine

kinetics were similar as expected (Figure S3B). In contrast, in the presence of the intradimeric wedge inhibitor nocodazole, which is thought to stabilize the curved conformation of tubulin, Eg5 nucleotide release was reduced more than fivefold (Figure 3F). This result is consistent with stabilization of the straight conformation of tubulin being coupled to nucleotide release by Eg5, which transitions the motor to the strong-binding state.

The coupling between tubulin straightening and Eg5 nucleotide turnover was also confirmed by solution ATPase assays. The tubulin-stimulated ATPase of $Eg5_M$ was well-described by a Michaelis-Menten curve with $K_M = 14.9 \pm 0.8$ μM and $k_{cat} = 1.5 \pm 0.04$ s^{-1} (Figure 3G, H). The intradimeric wedge inhibitor nocodazole reduced the ATP turnover rate by 7-fold ($K_M = 14.0 \pm 5$ μM, $k_{cat} = 0.2 \pm 0.03$ s^{-1}; Figure 3H). The identical x-intercepts (—$1/K_M$) in the Lineweaver-Burk plot indicate that nocodazole acts as a non-competitive inhibitor of the tubulin-stimulated $Eg5_M$ ATPase (Figure 3H). The data are consistent with the Eg5 chemomechanical cycle being tightly coupled to a conformational change (possibly a curved-to-straight transition) in tubulin that is blocked by nocodazole binding.

The L11-α4 junction mediates the slow motility, end-binding, and microtubule polymerase activity of Eg5

In kinesins, Switch II plays a key role in mechanochemical coupling between the nucleotide binding and microtubule binding sites [33]. In structures of tubulin-bound kinesin, the Loop11/helix 4 junction in Switch II (L11-α4) is positioned very close to the interface of alpha and beta tubulin (Figure 4A, S4A), placing it in the ideal location for detecting changes in tubulin curvature and sensing different conformations of tubulin in the lattice [17, 34]. Because Loop11 in the microtubule depolymerizing kinesin-8, Kip3, is necessary and sufficient for this motor's end-dwelling and microtubule depolymerase activities [11], we hypothesized that L11-α4 may be a distinguishing feature of Eg5 that confers the motor's microtubule polymerase activity.

To test this hypothesis, we swapped L11-α4 between the kinesin-1 KHC and Eg5 to create KHC_{swap} and $Eg5_{swap}$ (Figure 4B). Our first observation was that, in contrast to wild-type KHC, KHC swap accumulated at the plus-end of stabilized microtubules (Figure 4C). We next compared microtubule gliding velocities and found that, whereas wild-type KHC is 10-fold faster than Eg5, KHC_{swap} was 7-fold slower than $Eg5_{swap}$ (Figure 4D). The ATPase rate of KHC_{swap} fell proportionally to the stepping rate, indicating that the mutant retains tight coupling between ATP hydrolysis and stepping (Figure S4B and E). Previous work suggested that, whereas kinesin-1 spends half of its time in a one-head-bound state, Eg5 spends the bulk of its stepping cycle in a two-heads-bound state [22, 35, 36]. A biochemical analysis of transition rates in the mechanochemical cycle (Figure S4D–J) revealed that KHC_{swap} spends the bulk of its cycle in a two-heads-bound state, and $Eg5_{swap}$ becomes a one-head-bound motor.

We next tested the role of L11-α4 in microtubule nucleation, growth and stabilization. Adding Eg5 to free tubulin led to significantly more nucleated microtubules than KHC, but the L11-α4-swapped mutants flipped this relationship (Figure 4E, S4C). Microtubule shrinkage following tubulin washout was slowed three-fold by Eg5, whereas it was not affected by KHC; the relationship was flipped in the swap mutants (Figure 4F). Finally, Eg5

strongly enhanced and KHC only weakly enhanced the microtubule growth rate, and swapping the L11-α4 flipped this relationship (Figure 4G and H). In summary, the L11-α4 in Eg5 is necessary for end-binding, microtubule stabilization, and enhancement of microtubule growth, and swapping in the Eg5 L11-α4 is sufficient to confer these activities on the transport motor kinesin-1 (Cartoon in Figure S4I and J).

Effect of Eg5 on MT dynamics can be explained by a ~1 k_BT enhancement of lateral tubulin bond energy

To gain quantitative insight into how Eg5 alters microtubule dynamics, we carried out numerical simulations of microtubule growth and shortening using a previously developed Monte Carlo model [37]. In this formalism, tubulin incorporation at a growing plus-end involves formation of an initial longitudinal bond in one protofilament, followed by a curved-to-straight transition that triggers formation of a lateral bond with tubulin in any adjacent protofilaments (Figure 5A); shrinkage involves reversal of this pathway. Model parameters were taken from previous work or constrained by iterative fitting to our experimental data (Table S1). The model was able to recapitulate the experimental microtubule growth and shrinkage rates in the absence and presence of Eg5 motors (Figure 5B–E). Remarkably, the observed effects of Eg5 on microtubule dynamics can be quantitatively explained by Eg5 binding causing a 2.2-fold stabilization of the straight conformation of tubulin, equivalent to a 0.8 k_BT enhancement of tubulin-tubulin lateral binding energy (Table S2). Hence, our results are quantitatively consistent with a ‘Zippering’ model in which Eg5 binding straightens tubulin, which promotes tubulin-tubulin lateral bond formation, enhances the microtubule growth rate, and stabilizes the microtubule lattice against depolymerization (Figure 5F).

Discussion

We find that Eg5 dimers and monomers enhance microtubule nucleation, promote microtubule polymerization, and stabilize the microtubule lattice. Our results support a model in which Eg5 binding biases tubulin towards a straight conformation that promotes assembly. Thus, the role of Eg5 in the mitotic spindle likely goes beyond simply pushing apart anti-parallel microtubules, and may include maximizing the degree microtubule overlap in the midzone, driving poleward microtubule flux [38], and promoting aster formation during prometaphase [39].

Eg5 induces a curved-to-straight transition in tubulin that promotes polymerization

Because stability of the microtubule lattice results from the stabilizing energies of the lateral and longitudinal tubulin-tubulin contacts in the lattice [37, 40], driving tubulin toward the straight conformation promotes microtubule assembly by enabling lateral contacts to form. In contrast, tubulin wedge inhibitors like colchicine, nocodazole, and vinblastine decrease microtubule stability by stabilizing the kinked conformation of tubulin that is incompatible with lateral bond formation [6, 7, 30]. Our finding that Eg5 reduces the affinity of wedge inhibitors suggests that motor binding induces a straightening of tubulin (Figure 3C, D). If the curved-to-straight transition is treated as a rapid equilibrium, then in principle the polymerase activity could be achieved solely through stabilization of the (already formed)

straight conformation in the lattice. Consistent with this, our simulations suggest that only a subtle stabilization of the straight conformation is sufficient to explain all of the observed effects of Eg5 on microtubule dynamics (Figure 5). Also supporting this idea, a mutation in yeast tubulin that stabilizes the straight conformation was shown to decrease the microtubule shrinkage rate and catastrophe frequency, while having a negligible effect the tubulin on-rate [4]. Alternatively, Eg5 binding may trigger a curved-to-straight transition in tubulin. Eg5 actually had a higher apparent affinity for nocodazole-bound tubulin ($K_{0.5}$ of 21 μM and 9 μM for control and nocodazole, respectively; Figure 3F), suggesting that the motor binds readily to curved tubulin. Also, in ATPase assays, nocodazole decreased the tubulin-stimulated ATP turnover rate of Eg5 without changing the apparent tubulin affinity (Figure 3G and H). Thus, there is support for both Eg5 triggering a curved-to-straight transition and Eg5 simply stabilizing the straight conformation, and these two models are not mutually exclusive.

The long and flexible plus-end extensions seen on microtubules growing in the presence of Eg5 (Figure 1A) provide further evidence that Eg5 binding induces or stabilizes a curved-to-straight transition. In published electron micrographs, isolated protofilaments form curls and rings with diameters in the range of ~50 nm [3]; curvatures that are incompatible with lateral bond formation between protofilaments. A recent EM study found that splayed protofilaments with “ram’s horn” geometries are present not only in depolymerizing microtubules, but at the plus-ends of assembling microtubules as well [3]. The fact that plus-end curls observed here have diameters in the range of ~1 μm suggests that they are actually bundles of protofilaments stabilized by lateral contacts, like those seen on microtubule plus-ends by CryoEM [41]. These curved protofilaments suggest a two-step mechanism in which tubulin subunits are added to the end of growing protofilaments via longitudinal bonds, followed by a straightening step that forms lateral bonds. Eg5 localized at the plus-end promotes this straightening step.

Eg5 polymerase activity relies on a wedge-sensing structural element

Chemomechanical coupling in kinesins relies on the concerted movement of the Switch-I and Switch-II domains that surround the nucleotide binding pocket [42]. Upon ATP hydrolysis, closure of Switch-I displaces Switch-II and results in a weak-binding motor. Because Switch-II dictates the kinesin strong binding state, it is reasonable to predict that family-specific Switch-II sequences might define microtubule polymerase activity of kinesin.

In structures of kinesin bound to tubulin, the Loop11/helix 4 junction L11-α4, which lies just proximal to Switch-II, is located at the interface of the alpha and beta subunits of tubulin, the fulcrum around which tubulin bending occurs. We find that L11-α4 is the key family-specific sequence in kinesin-5 that confers its polymerase activity and that swapping in this sequence is sufficient to transform kinesin-1 into a polymerase. This finding provides a complement to the microtubule depolymerizing kinesin-8, Kip3, where the family-specific Loop11 was required for that motor’s microtubule depolymerase activity [11]. Recent cryoEM studies demonstrated that tubulin in the microtubule lattice is in a compact form in GDP, but takes on an extended form in GMPCPP or GDP + taxol, both of which stabilize the

lattice [28]. Shima and colleagues demonstrated that L11-α4 in kinesin-1 is involved in sensing the conformation of tubulin in the lattice, and that swapping in the corresponding sequence for kinesin-3 eliminates the ability to sense whether tubulin is in a compacted or expanded conformation [17]. Furthermore, it was shown that kinesin-1 binding to a compacted GDP lattice can trigger a transition to an extended lattice and enhance lattice stability as well [15, 17]. By analogy, in addition to its role in tubulin curvature, it is possible that Eg5 may also drive an expansion of the microtubule lattice and this effect may contribute to its microtubule stabilization activity.

Multi-modal regulatory mechanisms of tubulin assembly

By considering motor binding and tubulin assembly as a coupled equilibrium, a general model emerges that can describe the mechanisms of both polymerizing and depolymerizing motors. We found that Eg5 motor domain preferentially binds to microtubules over tubulin. In contrast, the depolymerizing kinesin-8, Kip3 preferentially binds to free tubulin [11] and the depolymerizing kinesin-13 preferentially binds to tubulin curls over straight tubulin in the lattice [43]. This thermodynamic model provides a general explanation for how other microtubule binding proteins may alter microtubule polymerization dynamics – those that bind more tightly to free tubulin promote depolymerization, whereas those that bind more tightly to the microtubule lattice promote polymerization. This mechanism may explain the recent report that kinesin-1 stabilizes GDP microtubules against depolymerization [15, 16]. A counter-example is the polymerase XMAP215, which preferentially binds curved, rather than straight tubulin [2]. However, its polymerase activity relies a different mechanism of capturing free tubulin subunits and delivering them to the growing plus end; and at low tubulin concentrations, XMAP215 accelerates microtubule depolymerization [44].

In summary, our results support a model in which Eg5 binding to a free tubulin dimer or to a curved protofilament induces a curved-to-straight transition that promotes lateral assembly of protofilaments into a stable microtubule lattice. In cells, the activity of full-length tetrameric Eg5 may be regulated by the motor's C-terminal tail, motor phosphorylation, as well as tubulin isoform differences and post-translational modifications. One general prediction is that any modification that preferentially enhances affinity of the Eg5 motor domain for tubulin polymer should lead to greater polymerase activity. The effect of Eg5 on microtubule stability is reminiscent to the effects of taxanes, opening a possible strategy for anticancer therapeutics that alters microtubule stability through effects on the Eg5 motor.

STAR Methods

CONTACT FOR REAGENT AND RESOURCE SHARING

Further information and requests for reagents may be directed to, and will be fulfilled by William O Hancock (wohbio@engr.psu.edu).

EXPERIMENTAL MODEL AND SUBJECT DETAILS

Eg5 dimers were generated by fusing the motor and neck linker domains (residues 1-368) of *Xenopus* kinesin-5 to the neck coil and coil 1 of KHC (residues 345-560), as previously described [21]. Monomeric Eg5 ($Eg5_M$) consisted of the head and neck linker (residues

1-368) of *Xenopus* kinesin-5 [22]. $Eg5_M$-GFP included an eGFP between the end of the neck linker domain and the start of the hexaHis tag. Unlabeled KHC was generated by truncating *Drosophila* kinesin-1 dimer (KHC) to sequence 1-406 and fusing to a C-terminal hexaHis tag. GFP-labeled kinesin-1 (KHC-GFP) consisted of residues 1-560 of KHC linked to C-terminal eGFP and hexaHis tag. The monomeric kinesin-1 construct (KHC_M) contains the head and neck linker domain (length 2-344) of KHC, preceded by an N-terminal hexaHis tag following the start codon [45]. For the identification of Loop11/Helix4 junction, kinesin-1, kinesin-5, and kinesin-8 sequences were compared using the Clustal Omega server (EMBL), according to the sequence identification published by Sablin *et al.* and Shima *et al.* [17, 46] (DmKHC: 239-256; XIEg5:259-276; residues are listed in Fig. S4A). To carry out domain-swapping, the primers with sequence of interest were synthesized (IDT) and introduced using the Q5 mutagenesis procedure (NEB). The kinesin-8 monomer ($KLP67A_M$) consists of the head and neck linker of *Drosophila* $KLP67A_{1-360}$. After PCR amplification, the linear DNAs were annealed using T4 ligase (NEB), followed by transformation into DH5α competent cells (NEB). All plasmids contain an ampicillin selection marker for antibiotic screening. All constructs were verified by sequencing (Penn State dnaTools).

Plasmids were transformed into E. coli BL21(DE3) for protein expression and grown in 2-liter cultures. Protein expression was induced by adding 1 mM IPTG and growing at 18 °C overnight. The collected pastes were resuspended into 25A200 buffer (25 mM K-ACES, pH 6.9, 2 mM Mg-Acetate, 2 mM K-EGTA, 0.1 mM K2-EDTA, 1 mM β-mercaptoethanol, 200 mM KCI, plus additional 10 μM ATP) and lysed by sonication. After Ni-column extraction, motors were exchanged into 0.5 μM mantADP with BRB80 buffer (80 mM PIPES, 1 mM EGTA, 1 mM $MgCl_2$, pH 6.8) using GE HiTrap Desalting column, followed by adding 10 vol% sucrose as cryo-protectant for flash-freeze in liquid N_2 before −80 °C storage. Detailed procedures for active motor quantification and yield optimization were described previously [47]. All experiments were performed in BRB80 buffer at 23-24 °C unless otherw ise noted.

PC-grade bovine brain tubulin was purified by three cycles of assembly and disassembly and labeled as described previously [48]. The labeled products were mixed with the unlabeled tubulin to generate aliquots of 5% Cy5-tubulin, 25% TMR-tubulin, and 5% biotinylated tubulin. GTP and Pi were removed by three additional assembly and disassembly rounds followed by buffer exchange into BRB80 plus 10 μM GDP. Tubulin concentrations were calculated by absorbance using an extinction coefficient ε_{280} = 115,000 $M^{-1}cm^{-1}$.

METHOD DETAILS

All experiments were carried out in BRB80 buffer (80 mM K-PIPES, 1 mM EGTA, 1 mM $MgCl_2$, pH 6.8) plus added components.

Microtubule gliding assays.—40 μM TMR-labeled tubulin, 8 vol% DMSO, and 2 mM Mg-GTP were incubated at 37°C and stabilized by adding 10 μM taxol. Motor gliding velocities of surface-adsorbed kinesin motors were imaged by TMR-labeled taxol-stabilized microtubules and quantified by MtrackJ plugin of ImageJ, as previously described [27].

Unless otherwise indicated, the assays were carried out in imaging solution of BRB80 plus oxygen scavenger system and 0.2 mg/mL casein at 22 °C [27].

Microtubule counting and template nucleation assays.—Methods are based on protocols published by the Mitchison group [24], with the conditions adapted for fluorescent microscope visualization. TMR-labeled tubulin was incubated with 10 vol% DMSO plus 2 mM Mg-GTP in the presence or absence of kinesin motors plus 5 mM ATP at 37°C for 10 minutes to generate microtubule seeds. The nucleated products were diluted 10-fold in imaging solution plus 10 μM taxol at 22°C for 1 hour to elongate pre-formed seeds and minimize the *de novo* seed formation. The resulting solutions were diluted into imaging buffer plus 5 mM ATP and bound to the surface coated with 100 nM kinesin-1 rigor mutants for 20 minutes. The surface-bound microtubules with length >1 μm were scored.

Following a protocol developed by the Brouhard group [25], TMR-labeled free tubulin was added with 5 mM Mg-ATP and 2 mM Mg-GTP and then incubated with surface-immobilized GMPCPP-seeds at 37 °C for 15 minutes. The reaction was quenched by tubulin washout using the imaging solution plus 10 μM taxol. Nucleation events were scored on the basis of the visibility of newly formed polymer at the end of templates, and the fractions of nucleation were fit a Hill equation in the presence or absence of Eg5 treatment.

Microtubule dynamics and shrinkage assays.—To form GMPCPP-seeds, 2 μM tubulin total (0.1 μM Cy5-labeled + 0.1 μM biotinylated + 1.8 μM unlabeled tubulin) were mixed with 0.2 mM Mg-GMPCPP at 37°C for 5 hours, followed by one spin-an d-resuspension cycle to remove free tubulin. Coverslips were rinsed three times with 70% ethanol, followed by overnight acid cleaning in 6 M HCI. Acid-cleaned coverslips were rinsed by ddH_2O, subjected to plasma cleaning (Harrick Plasma) for 2 minutes, incubated in vacuum-based dessicator with silane-vapor (Abeam) for at least 2 hours, and finally fixed by two pieces of double-sided tape to generate silanized flow chambers. To immobilize Cy5-labeled seeds, 500 nM neutravidin (Thermo Scientific), 5 wt% Pluronic F108 (BASF Corp.) 2 mg/mL casein were flowed in sequentially in intervals.

Polymerization was initiated by combining TMR-labeled tubulin, 5 mM Mg-ATP, and 2 mM Mg-GTP in the presence or absence of kinesin motors. For most microtubule dynamics assays, the entire polymerization process was visualized under Nikon TE-2000 TIRF microscope, as previously described [21]. A subset of microtubule dynamics assays using unlabeled tubulin employed Interference Reflection Microscopy at 25°C, following previously described protocols [49][50]; those assays used 0.2% methyl cellulose to help keep microtubules near the glass surface. Microtubule growth velocities were measured by linear fit of kymographs using ImageJ software, where the fast-growing ends were defined as the plus-ends. For microtubule shrinkage assays, polymerization was carried out on a 37°C heat plate for 20 minutes, and catastrophe induced by flowing through room-temperature (22°C) tubulin-free buffer. For experiments in presence of motors, motor concentrations in polymerization solution and shrinkage solution were identical to maintain motor-microtubule interactions both before and after catastrophe. The entire process was carried out on stage using epi-fluorescence microscope, as previously described [48]. Shrinkage velocities were quantified using the ImageJ plugin, MtrackJ. Both assays were

carried out in imaging solution of BRB80 plus oxygen scavenger system and 0.2 mg/mL casein, as we used for microtubule gliding assays.

Kinesin tip-dwelling assays.—Both Cy5-labeled GMPCPP-stabilized microtubules and Cy5-labeled taxol-stabilized microtubules were tested for motor tip-dwelling. To reach the steady-state end-bulbs, the GFP-labeled kinesin motors were incubated in the flow chamber for 10-15 minutes before image acquisition.

Turbidity assays.—Polymer formation was induced by mixing unlabeled tubulin plus 10 vol% DMSO, 2 mM Mg-GTP, 5 mM ATP at 37 °C, in the presence or absence of motors. Turbidity signals were recorded at 340 nm on a Multi-Mode Micro Plate Reader (Molecular Device Flexstation 3). The resulting traces were sigmoidal, corresponding to an initial nucleation phase followed by extension phase.

Steady-state ATPase assays.—Tubulin-stimulated ATPase rates were measured using the EnzChek phosphatase assay kit (Molecular probes, ThermoFisher Scientific) at 22 °C. In solutions, 0.5 mM GDP and 3 mM ATP were used to avoid ATP-triggered tubulin polymerization. Microtubule-induced ATPase rates were carried out by enzyme-coupled assays with 5-20 nM active motors using a Multi-Mode Micro Plate Reader (Molecular Devices Flexstation 3), as previously described [27]. Data are presented as mean ± s.e.m. for N = 3 determinations for each point, and fit with a Michaelis-Menten equation to obtain the maximal rate k_{cat} and the half-max concentration K_M.

Demecolcine-binding affinity and colchicine-binding kinetics.—2 μM tubulin was first incubated with 3.5 μM kinesin motors plus nucleotides for 30 minutes, and then this tubulin-kinesin complex was mixed with varying concentrations of the colchicine analog, demecolcine, for the next 1 hour. This step ensures the tubulin being completely bound to kinesin motors. Upon demecolcine binding, the quenching of tubulin intrinsic fluorescence at Ex 280 nm/Em 346 nm provides a simple method to quantify binding fraction of demecolcine on tubulins. For colchicine-binding kinetics, 5 μM tubulin was first incubated with AMPPNP-bound Eg5 monomers for 30 minutes, followed by adding 50 μM colchicine and recording the tubulin-induced colchicine fluorescence signal (Ex 366 nm/Em 435 nm). Traces were fit to a biexponential.

Stopped flow experiments.—Stopped-flow assays were performed on an Applied Physics SX20 spectrofluorometer at 22 °C, as previously describe d [47]. Free tubulin was first incubated with 1.2× wedge inhibitors for 1 hour, and then flushed against 0.2 μM mantADP-bound Eg5 monomers. Upon tubulin binding, Eg5 motors release mantADP and result in a signal drop. Traces were fit to a mono-exponential to obtain the observed rate constants. Across varying tubulin concentrations, the observed rate constants follow the function,

$$k_{obs} = \frac{[Tubulin]}{[Tubulin] + K_{0.5}} k_{off} .$$

where k_{off} and $K_{0.5}$ denotes the ADP off-rate and the apparent MT affinity, respectively.

Simulation of microtubule dynamics.—Because tubulin has a kinked conformation in solution [1, 2], two consecutive steps were included for tubulin incorporation into the lattice: longitudinal bond formation and lateral bond formation [37]. Lateral bond formation implicitly includes the curved-to-straight transition and lateral bond breakage implicitly includes the straight-to-curved transition. Simulations started from a 13:2 seed that did not include a seam. The model required eight parameters to define microtubule dynamics: the tubulin-tubulin longitudinal on-rate (k_{on}, $\mu M^{-1}s^{-1}$ per MT), the tubulin hydrolysis rate (k_{hyd}, s^{-1}), the longitudinal tubulin off-rates in GTP (k_{off}^{GTP}, s^{-1}) and GDP (k_{off}^{GDP}, s^{-1}), the forward and reverse lateral bond annealing rates (k_{zip} and k_{unzip}, s^{-1}), and stabilization factors for both GTP tubulin (F_{GTP}, fold) and the mechanical stabilization by the microtubule lattice (F_{wall}, fold). To characterize microtubule shrinkage, the tubulin hydrolysis rate was set to either 50 s' or 0 s^{-1} to approximate GDP- or GMPCPP-tubulin, respectively; other parameters for growing microtubules are given in Table S1. To simulate microtubule growth and shortening in the presence of Eg5 motors, a further seven experimentally-derived [21, 22] or -constrained parameters were assigned: the Eg5 on-rate (k_{on}^{Motor}, $\mu M\ MT^{-1}s^{-1}$), the Eg5 stepping rate on the lattice (k_{step}, s^{-1}) and on curved protofilaments (k_{slow}, s^{-1}), the Eg5 unbinding rate from the lattice (k_{unbind}, s^{-1}) and from curved protofilaments (k_{pause}, s^{-1}), a factor for the enhancement of lateral bond formation by Eg5 (k_{zip}^{Eg5}, s^{-1}), and a factor for the stabilization of lateral bonds by Eg5 (k_{unzip}^{Eg5}, fold). The free energies resulting from these kinetic parameters are presented in Table S2.

Structural superposition.—Structures of Eg5-tubulin complex (PDB: 4AQW) and inhibitor-bound tubulins were aligned on the basis of α-tubulins (colchicine, PDB: 4O2B; nocodazole, PDB: 5CA1; Maytansinoid DM1, PDB: 4TV8) and visualized by UCSF Chimera.

QUANTIFICATION AND STATISTICAL ANALYSIS

Data were fit in OriginPro 9.1 software. Microtubule dynamics were simulated by MATLAB R2017b. Unless otherwise indicated, data are presented as mean ± SEM. Detailed statistical information can be found in Figure Legends.

DATA AND SOFTWARE AVAILABILITY

Requests for simulation codes may be directed to, and will be fulfilled by William O Flancock (wohbio@engr.psu.edu).

Supplementary Material

Refer to Web version on PubMed Central for supplementary material.

Acknowledgments

This work was supported by NIH R01 GM076476 and NIH R01 GM100076 to W.O.H. and R01 GM113164 to H.S. J.M.C. was supported by NIH T32 GM108563. A portion of the bacterial culture work was carried out at the Penn State Huck Institutes for Life Sciences Fermentation Facility with the assistance of M. Signs. The authors thank

Dan Sackett (NIH), David Sept (UMich), Luke Rice (UT Southwestern), Gary Brouhard (McGill), and John Correia (UMC) for thoughtful discussions on tubulin wedge inhibitors and tubulin curvature-sensing mechanisms.

References

1. Rice LM, Montabana EA, and Agard DA (2008). The lattice as allosteric effector: structural studies of alphabeta- and gamma-tubulin clarify the role of GTP in microtubule assembly. Proc. Natl. Acad. Sci. 105, 5378–83. [PubMed: 18388201]
2. Ayaz P, Ye X, Fluddleston P, Brautigam CA, and Rice LM (2012). A TOG : αβ-tubulin Complex Structure. Science 337, 857–60. [PubMed: 22904013]
3. McIntosh JR, Toole EO, Morgan G, Austin J, Ulyanov E, Ataullakhanov F, and Gudimchuk N (2018). Microtubules grow by the addition of bent guanosine triphosphate tubulin to the tips of curved protofilaments. J. Cell Biol. 217, 2691–2708. [PubMed: 29794031]
4. Geyer EA, Burns A, Lalonde BA, Ye X, Piedra FA, Fluffaker TC, and Rice LM (2015). A mutation uncouples the tubulin conformational and GTPase cycles, revealing allosteric control of microtubule dynamics. Elife 4, 1–20.
5. Ti SC, Pamula MC, Howes SC, Duellberg C, Cade NI, Kleiner RE, Forth S, Surrey T, Nogales E, and Kapoor TM (2016). Mutations in Human Tubulin Proximal to the Kinesin-Binding Site Alter Dynamic Instability at Microtubule Plus- and Minus-Ends. Dev. Cell 37, 72–84. [PubMed: 27046833]
6. Ravelli RBG, Gigant B, Curmi PA, Jourdain I, Lachkar S, Sobel A, and Knossow M (2004). Insight into tubulin regulation from a complex with colchicine and a stathmin-like domain. Nature 428, 198–202. [PubMed: 15014504]
7. Gigant B, Wang C, Ravelli RBGG, Roussi F, Steinmetz MO, Curmi PA, Sobel A, and Knossow M (2005). Structural basis for the regulation of tubulin by vinblastine. Nature 435, 519–522. [PubMed: 15917812]
8. Varga V, Helenius J, Tanaka K, Hyman AA, Tanaka TU, and Howard J (2006). Yeast kinesin-8 depolymerizes microtubules in a length-dependent manner. Nat. Cell Biol. 8, 957–962. [PubMed: 16906145]
9. Varga V, Leduc C, Bormuth V, Diez S, and Howard J (2009). Kinesin-8 Motors Act Cooperatively to Mediate Length-Dependent Microtubule Depolymerization. Cell 138, 1174–1183. [PubMed: 19766569]
10. Helenius J, Brouhard G, Kalaidzidis Y, Diez S, and Howard J (2006). The depolymerizing kinesin MCAK uses lattice diffusion to rapidly target microtubule ends. Nature 441, 115–119. [PubMed: 16672973]
11. Arellano-Santoyo H, Geyer EA, Stokasimov E, Chen G-Y, Su X, Hancock W, Rice LM, and Pellman D (2017). A Tubulin Binding Switch Underlies Kip3 / Kinesin-8 Depolymerase Activity. Dev. Cell 42, 37–51. [PubMed: 28697331]
12. Wang D, Nitta R, Morikawa M, Yajima H, Inoue S, Shigematsu H, Kikkawa M, and Hirokawa N (2016). Motility and microtubule depolymerization mechanisms of the Kinesin-8 motor, KIF19A. Elife 5, 1–24.
13. Benoit MPMH, Asenjo AB, and Sosa H (2018). Cryo-EM reveals the structural basis of microtubule depolymerization by kinesin-13s. Nat. Commun. 9, 1662. [PubMed: 29695795]
14. Gudimchuk N, Vitre B, Kim Y, Kiyatkin A, Cleveland DW, Ataullakhanov FI, and Grishchuk EL (2013). Kinetochore kinesin CENP-E is a processive bi-directional tracker of dynamic microtubule tips. Nat. Cell Biol. 15, 1079–1088. [PubMed: 23955301]
15. Peet DR, Burroughs NJ, and Cross RA (2018). Kinesin expands and stabilizes the GDP-microtubule lattice. Nat. Nanotechnol. 13, 386–391. [PubMed: 29531331]
16. Reuther C, Diego AL, and Diez S (2016). Kinesin-1 motors can increase the lifetime of taxol-stabilized microtubules. Nat. Nanotechnol. 11, 914–915. [PubMed: 27821845]
17. Shima T, Morikawa M, Kaneshiro J, Kambara T, Kamimura S, Yagi T, Iwamoto H, Uemura Sotaro, Shigematsu H, Shirouzu M, et al. (2018). Kinesin-binding-triggered conformation switching of microtubules contributes to polarized transport. J. Cell Biol. 217, 4164–83. [PubMed: 30297389]

18. Gardner MK, Bouck DC, Paliulis LV, Meehl JB, O'Toole ET, Haase J, Soubry A, Joglekar AP, Winey M, Salmon ED, et al. (2008). Chromosome Congression by Kinesin-5 Motor-Mediated Disassembly of Longer Kinetochore Microtubules. Cell 135, 894–906. [PubMed: 19041752]
19. Fridman V, Gerson-Gurwitz A, Shapira O, Movshovich N, Laka S, Schmidt CF, Gheber L, Lakamper S, Schmidt CF, and Gheber L (2013). Kinesin-5 Kip1 is a bi-directional motor that stabilizes microtubules and tracks their plus-ends in vivo. J. Cell Sci. 126, 4147–59. [PubMed: 23868978]
20. Rincon SA, Lamson A, Blackwell R, Syrovatkina V, Fraisier V, Paoletti A, Betterton MD, and Tran PT (2017). Kinesin-5-independent mitotic spindle assembly requires the antiparallel microtubule crosslinker Ase1 in fission yeast. Nat. Commun. 8, 15286. [PubMed: 28513584]
21. Chen Y, and Hancock WO (2015). Kinesin-5 is a microtubule polymerase. Nat. Commun. 6, 8160. [PubMed: 26437877]
22. Chen G-Y, Mickolajczyk KJ, and Hancock WO (2016). The Kinesin-5 Chemomechanical Cycle is Dominated by a Two-heads-bound State. J. Biol. Chem. 291, 20283–20294. [PubMed: 27402829]
23. Roostalu J, and Surrey T (2017). Microtubule nucleation: beyond the template. Nat. Rev. Mol. Cell Biol. 18, 702–710. [PubMed: 28831203]
24. Zheng Y, Wong ML, Alberts B, and Mitchison TJ (1995). Nucleation of microtubule assembly by a γ-tubulin-containing ring complex. Nature 378, 578–583. [PubMed: 8524390]
25. Wieczorek M, Bechstedt S, Chaaban S, and Brouhard GJ (2015). Microtubule-associated proteins control the kinetics of microtubule nucleation. Nat. Cell Biol. 17, 907–16. [PubMed: 26098575]
26. Cochran JC, Sontag CA, Maliga Z, Kapoor TM, Correia JJ, and Gilbert SP (2004). Mechanistic analysis of the mitotic kinesin Eg5. J. Biol. Chem. 279, 38861–38870. [PubMed: 15247293]
27. Chen G-Y, Kang YJ, Gayek AS, Youyen W, TOzel E, Ohi R, and Hancock WO (2017). Eg5 Inhibitors Have Contrasting Effects on Microtubule Stability and Metaphase Spindle Integrity. ACS Chem. Biol. 72, 1038–1046.
28. Alushin GM, Lander GC, Kellogg EH, Zhang R, Baker D, and Nogales E (2014). High-Resolution microtubule structures reveal the structural transitions in αβ-tubulin upon GTP hydrolysis. Cell 157, 1117–1129. [PubMed: 24855948]
29. Akhmanova A, and Steinmetz MO (2015). Control of microtubule organization and dynamics: two ends in the limelight. Nat. Rev. Mol. Cell Biol. 16, 711–26. [PubMed: 26562752]
30. Wang Y, Zhang H, Gigant B, Yu Y, Wu Y, Chen X, Lai Q, Yang Z, Chen Q, and Yang J (2016). Structures of a diverse set of colchicine binding site inhibitors in complex with tubulin provide a rationale for drug discovery. FEBS J. 283, 102–111. [PubMed: 26462166]
31. Pyles EA, and Hastie SB (1993). Effect of the B Ring and the C-7 Substituent on the Kinetics of Colchicinoid-Tubulin Associations. Biochemistry 32, 2329–2336. [PubMed: 8443174]
32. Lambeir A, and Engelborghs Y (1981). A fluorescence stopped flow study of colchicine binding to tubulin. J. Biol. Chem. 256, 3279–3282. [PubMed: 7204403]
33. Kull FJ, and Endow SA .(2002). Kinesin: switch I & II and the motor mechanism. J. Cell Sci. 115, 15–23. [PubMed: 11801720]
34. Gigant B, Wang W, Dreier B, Jiang Q, Pecqueur L, PlOckthun A, Wang C, and Knossow M (2013). Structure of a kinesin-tubulin complex and implications for kinesin motility. Nat. Struct. Mol. Biol. 20, 1001–7. [PubMed: 23872990]
35. Mickolajczyk KJ, Deffenbaugh NC, Arroyo JO, Andrecka J, Philipp K, and Hancock WO (2015). Kinetics of nucleotide-dependent structural transitions in the kinesin-1 hydrolysis cycle. Proc. Natl. Acad. Sci. 112, E7186–93. [PubMed: 26676576]
36. Andreasson JOL, Milic B, Chen G-Y, Guydosh NR, Hancock WO, and Block SM (2015). Examining kinesin processivity within a general gating framework. Elife 4, e07403.
37. Margolin G, Gregoretti IV, Cickovski TM, Li C, Shi W, Alber MS, and Goodson HV (2012). The mechanisms of microtubule catastrophe and rescue: implications from analysis of a dimer-scale computational model. Mol. Biol. Cell 23, 642–656. [PubMed: 22190741]
38. Miyamoto DT, Perlman ZE, Burbank KS, Groen AC, and Mitchison TJ (2004). The kinesin Eg5 drives poleward microtubule flux in Xenopus laevis egg extract spindles. J. Cell Biol. 167, 813–818. [PubMed: 15583027]

39. Helmke KJ, and Heald R (2014). TPX2 levels modulate meiotic spindle size and architecture in Xenopus egg extracts. J. Cell Biol. 206, 385–393. [PubMed: 25070954]
40. Gardner MK, Charlebois BD, Janosi IM, Howard J, Hunt AJ, and Odde DJ (2011). Rapid microtubule self-assembly kinetics. Cell 146, 582–592. [PubMed: 21854983]
41. Atherton J, Stouffer M, Francis F, and Moores CA (2018). Microtubule architecture in vitro and in cells revealed by cryo-electron tomography. Acta Crystallogr. D. Biol. Crystallogr. 74, 572–584.
42. Nitta R, Okada Y, and Hirokawa N (2008). Structural model for strain-dependent microtubule activation of Mg-ADP release from kinesin. Nat. Struct. Mol. Biol. 15, 1067–1075. [PubMed: 18806800]
43. Friel CT, and Howard J (2011). The kinesin-13 MCAK has an unconventional ATPase cycle adapted for microtubule depolymerization. EMBO J. 30, 3928–3939. [PubMed: 21873978]
44. Brouhard GJ, Stear JH, Noetzel TL, Al-Bassam J, Kinoshita K, Harrison SC, Howard J, and Hyman AA (2008). XMAP215 Is a Processive Microtubule Polymerase. Cell 132, 79–88. [PubMed: 18191222]
45. Shastry S, and Hancock WO (2011). Interhead tension determines processivity across diverse N-terminal kinesins. Proc. Natl. Acad. Sci. 108, 16253–16258. [PubMed: 21911401]
46. Sablin E, Kull F, Cooke R, Vale R, and Fletterick R (1996). Crystal structure of the motor domain of the kinesin-related motor nod. Nature 380, 555–559. [PubMed: 8606780]
47. Chen G-Y, Arginteanu DFJ, and Hancock WO (2015). Processivity of the Kinesin-2 KIF3A Results From Rear-Head Gating and Not Front-Head Gating. J. Biol. Chem. 290, 10274–10294. [PubMed: 25657001]
48. Uppalapati M, Huang Y, Shastry S, Jackson TN, and Hancock WO (2009). Microtubule Motors in Microfluidics In Methods in Bioengineering: Microfabrication and Microfluidics, Lee LP and Zahn JD, eds. (Boston, MA: Artech House Publishers), pp. 311–337.
49. Simmert S, Abdosamadi MK, Hermsdorf G, and Schaffer E (2018). LED-based interference-reflection microscopy combined with optical tweezers for quantitative three-dimensional microtubule imaging. Opt. Express 26, 14499–513. [PubMed: 29877486]
50. Mahamdeh M, Simmert S, Luchniak A, Schaffer E, and Howard J (2018). Label-free high-speed wide-field imaging of single microtubules using interference reflection microscopy. J. Microsc. 272, 60–66. [PubMed: 30044498]

Highlights:

- Eg5 motor domain is sufficient to promote microtubule nucleation and assembly.
- Eg5 binding to tubulin promotes curved-to-straight transition.
- Eg5 binding and microtubule assembly can be treated as coupled equilibria.
- Loop11/α4 junction is necessary and sufficient for polymerase activity.

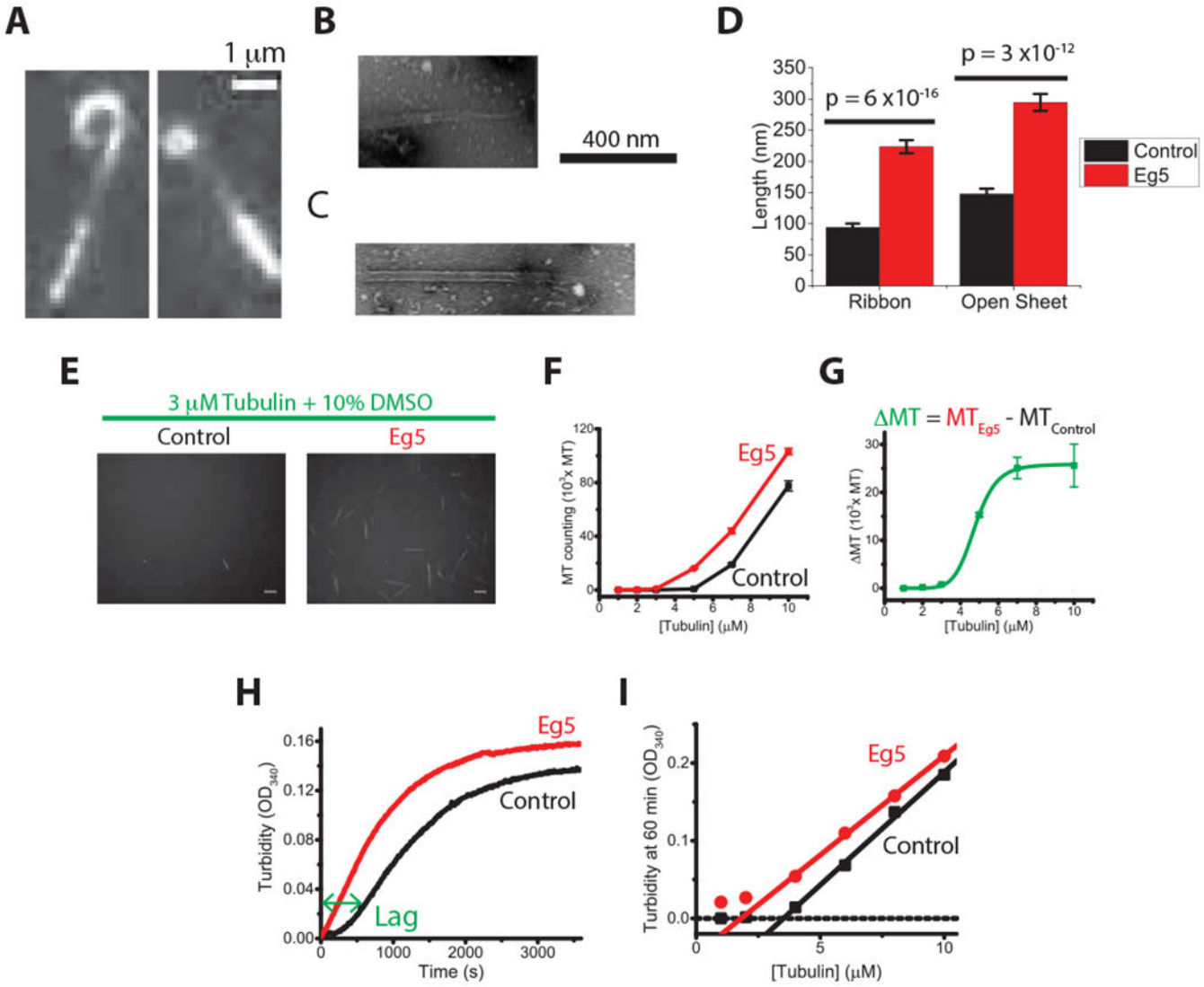

Figure 1. Eg5 motors enhance microtubule nucleation and growth.

(A) TIRF microscopy images of dynamic microtubule plus-ends growing in the presence of GFP-labeled dimeric Eg5. See also Video S1 and S2. (B and C) Negative-stain EM image of microtubules grown in the presence of Eg5, showing ribbon (B) and sheet (C) structures (see Figure S1 for more examples). (D) Quantification of the length of ribbons and open sheets in the presence and absence of dimeric Eg5 motors (mean ± SEM; n_{MT} = 243–315; ribbon lengths, $p = 6 \times 10^{-16}$; open sheet lengths, $p = 3 \times 10^{-12}$). (See Figure S1 for length distributions and frequencies.) (E) Epi-fluorescence images of TMR-labeled microtubules nucleated and grown at 37 °C in the presence or absence of unlabeled Eg5 dimers (mean ± SEM; n = 10). Scale bar: 5 μm. (F and G) Number of nucleated microtubules as a function of initial free tubulin concentration. (H) Averaged turbidity traces of 8 μM free tubulin plus 10% DMSO growing at 37°C in the presence and absence of 130 nM Eg5 motors, demonstrating that Eg5 reduces nucleation lag time and results in higher turbidity plateau (n = 3-5 traces). (I) Turbidity signal at 1 hour across tubulin concentrations, demonstrating that Eg5 reduces critical concentration of tubulin nucleation. See also Figure S1.

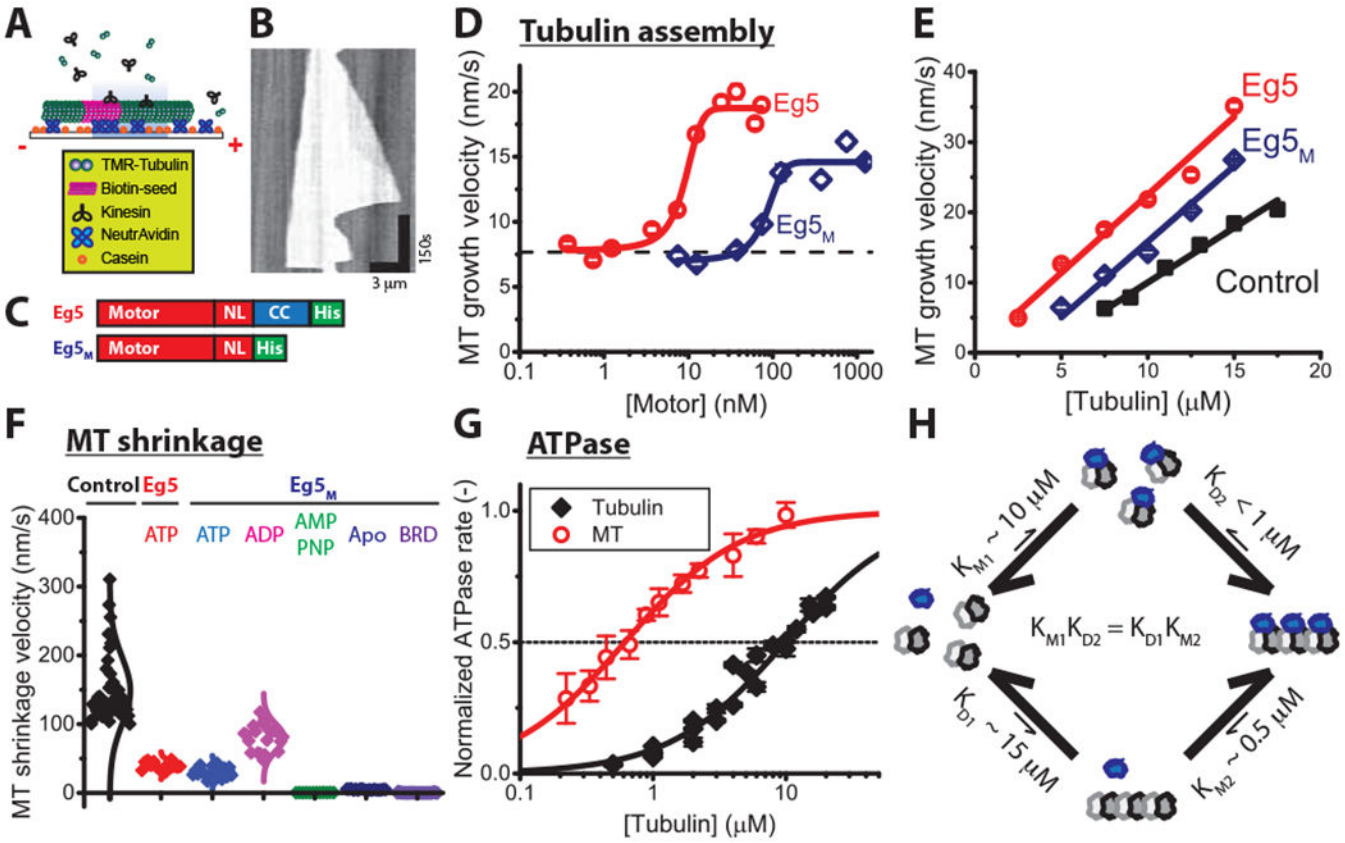

Figure 2. Monomeric Eg5 promotes microtubule assembly and enhances microtubule stability.

(A-E) Microtubule growth rates. (A) Schematic of microtubule dynamics assays, in which free tubulin is grown off of biotinylated GMPCPP microtubule seeds. (B) Example kymograph showing unlabeled seed and growth from both ends over time, visualized by Interference Reflection Microscopy. (C) Diagrams of constructs. Dimeric Eg5 was made by replacing the native Eg5 coiled-coil with the kinesin-1 coiled-coil to ensure stable dimerization [21, 45]. (D) Motor-dependent microtubule growth velocities at 7.5 μM tubulin and varying motor concentrations at 25 °C (mean ± SEM; n_{MT} = 47-291 for Eg5 and 11-147 for $Eg5_M$). (E) Tubulin-dependent microtubule elongation rates at saturating motor concentrations (61 nM Eg5 and 1.25 μM $Eg5_M$; mean ± SEM; n_{MT} = 53-114, 62-142, and 37-427 for control, Eg5 and $Eg5_M$, respectively). (F) Effects of Eg5 on microtubule shrinkage rates following tubulin washout at 22 °C, visualized by TIRF microscopy. Dimeric Eg5 was used at 80 nM and monomeric $Eg5_M$ was used at 10 μM under different nucleotide conditions (n_{MT} = 12-42). (G) Tubulin- and microtubule-stimulated ATPase of monomeric Eg5 at 22 °C. ATPase rates are normalized to maximal for each substrate. Based on the K_M values, the apparent affinity of $Eg5_M$ for tubulin (K_{M1} = 9.9 ± 1.2 μM) is 20-fold lower than its affinity for microtubules (K_{M2} = 0.6 ± 0.03 μM), which suggests that Eg5 motors favor the straight conformation of tubulin (mean ± SEM; n_{MT} = 5; n_{Tub} = 3). Mean ± SEM. (H) Schematic of affinity-driven polymer assembly. The twenty-fold difference of Eg5 affinity in Figure 2G generates a potential to facilitate tubulin assembly, consistent with the differential critical concentrations of microtubule growth in the presence and absence of monomeric Eg5 in Figure 2E. See also Figure S2.

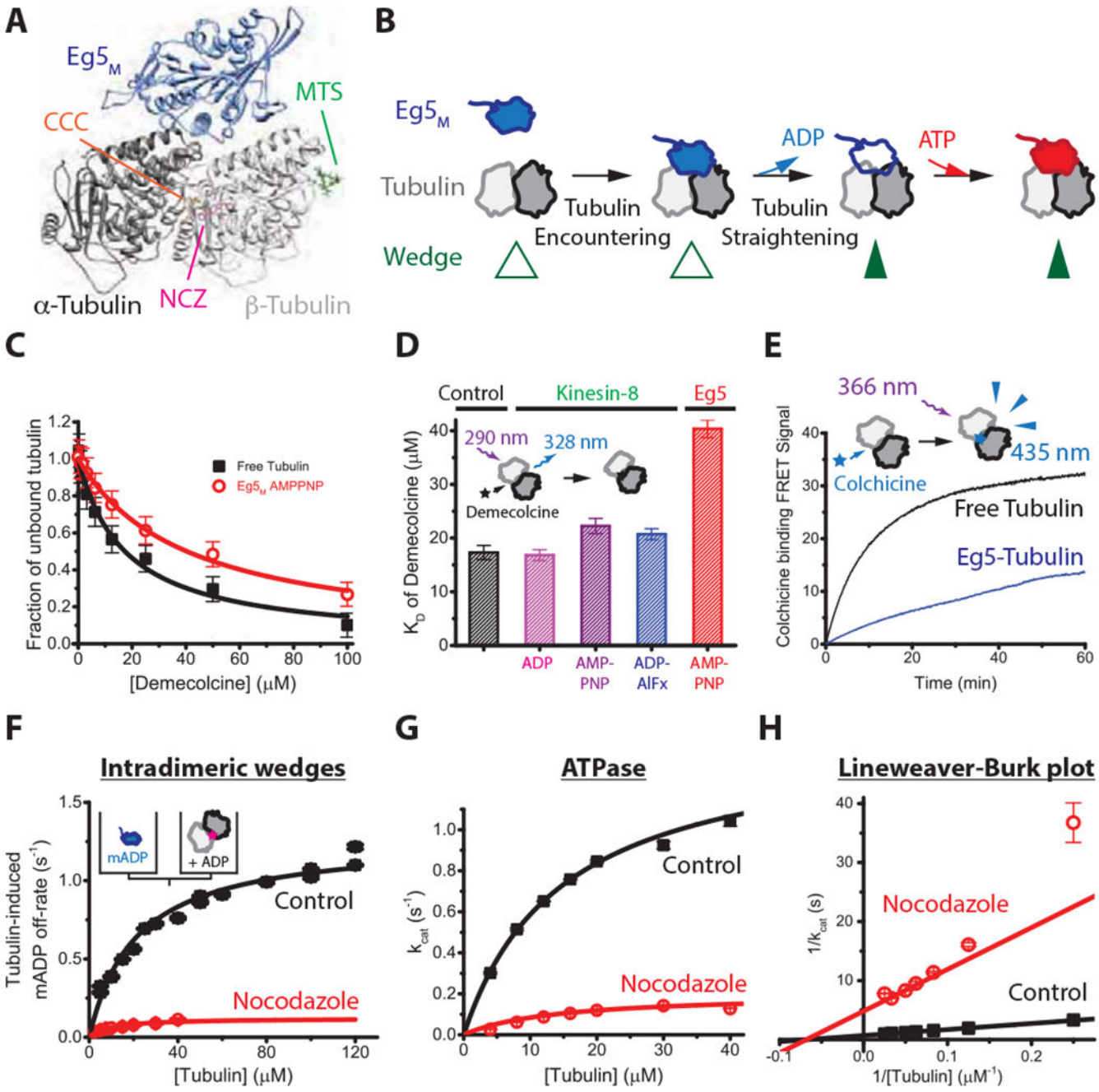

Figure 3. Eg5-binding causes a structural change that promotes tubulin assembly.

(A) Structure of Eg5 motor domain bound to free tubulin (PDB: 4AQW) and binding sites for inter- and intradimer wedge inhibitors. CCC, colchicine (PDB: 4O2B); NCZ, Nocodazole (PDB: 5CA1); MTS, Maytansinoid DM1 (PDB: 4TV8). (B) Model of coupling between nucleotide turnover in Eg5 and straightening of tubulin. Motor binding to free tubulin triggers ADP release, which causes a weak-to-strong binding transition that stabilizes the straight conformation of tubulin; ATP binding and hydrolysis follow. (C) Demecolcine binding assays based on quenching of tubulin autofluorescence by drug binding at 22 °C. Data were fit by a binding isotherm, yielding K_D of 17 ± 1.3 μM for

control and K_D of 40 ± 1.6 μM in the presence of 4 μM $Eg5_M$ and 1 mM AMPPNP that induces the strong-binding state of the motor. (D) K_D for Demecolcine-tubulin binding, including results for the monomeric kinesin-8 $KLP67A_M$ across various nucleotide-states; see Figure S3A for details. (E) Kinetics of 50 μM colchicine binding to 5 μM tubulin in the presence or absence of AMPPNP-bound motors. Biexponential fit to control yielded fast and slow phases with rates and amplitudes of 0.169 ± 0.004 s^{-1} and 14 A.U., and 0.048 ± 0.001 s^{-1} and 19 A.U., respectively. In Eg5, fast and slow phases were 0.201 ± 0.022 s^{-1} and 1 A.U., and 0.0085 ± 0.0006 s^{-1} and 32 A.U., respectively. (F) Tubulin-induced mantADP release at 22 °C. Eg5 monomers pre-loaded with mantADP were flushed against tubulin pre-incubated with wedge inhibitors, and the resulting fluorescence fall due to mantADP release fit to a falling exponential. First-order rate constants where plotted across varying tubulin concentrations and fit to hyperbola to obtain the maximal ADP release rate, k_{max}, and the tubulin concentration for half-maximal release, $K_{0.5}$. Control: $K_{0.5}$ = 21 ± 8 μM, k_{max} = 1.3 ± 0.2 s^{-1}; Nocodazole: $K_{0.5}$ = 9 ± 13 μ M; k_{max} = 0.12 ± 0.06 s^{-1} (n = 5-7 for each averaged trace; mean ± SEM). (G and H) Tubulin-stimulated $Eg5_M$ ATPase in the presence or absence of the intra-dimeric wedge inhibitor, nocodazole, at 22 C°. Control: k_{cat} of 1.46 ± 0.04 s^{-1} and K_M of 14.9 ± 0.8 μM tubulin; nocodazole: k_{cat} of 0.20 ± 0.03 s^{-1} and K_M of 14 ± 5 μM tubulin; n = 3; mean ± SEM). See also Figure S3.

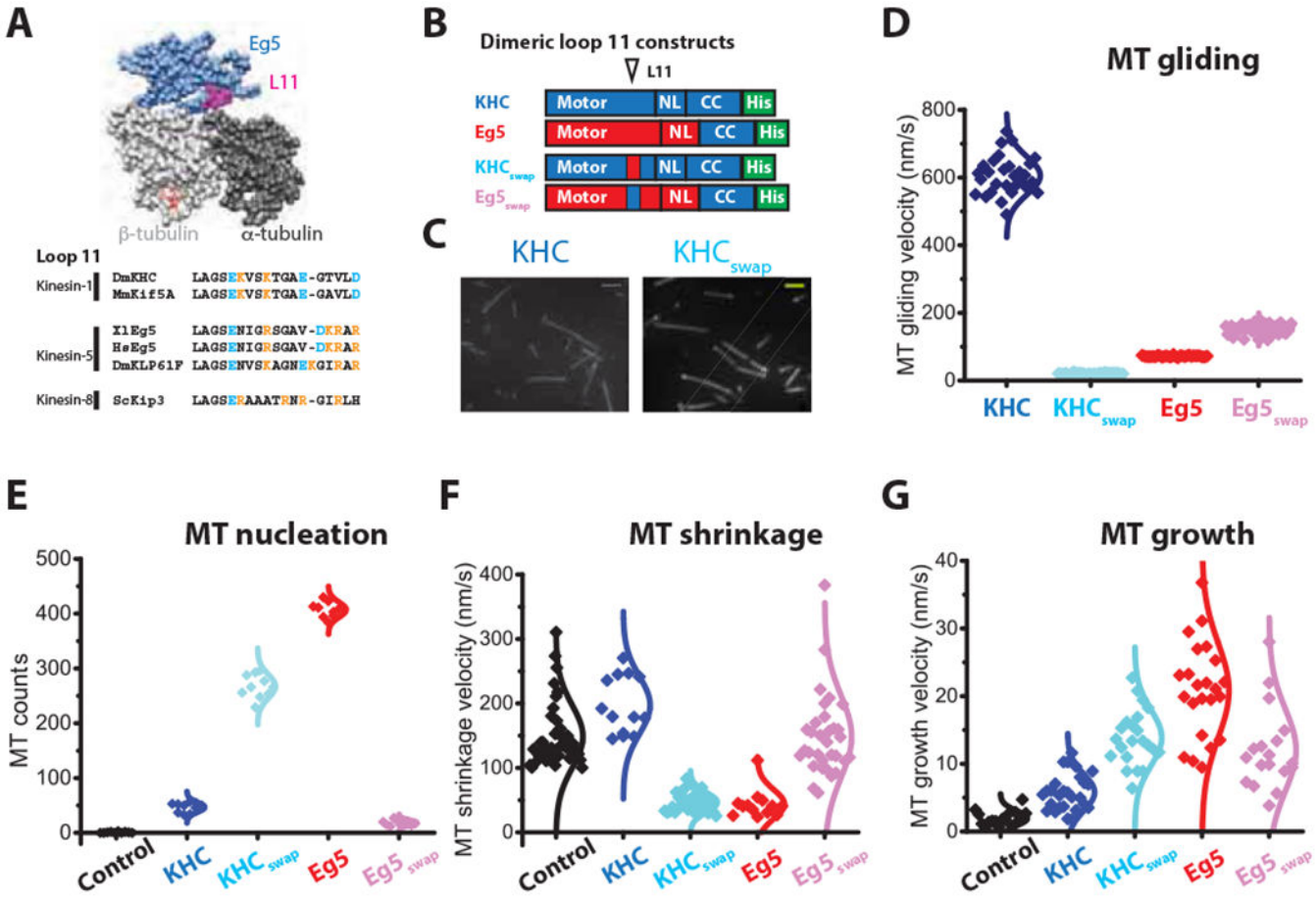

Figure 4. Loop11-helix 4 mediates Eg5 end-accumulation and microtubule polymerase activity.

(A) Structure of tubulin-bound Eg5, highlighting the location of L11-α4 at the α/β-tubulin interface (PDB: 4AQW). Comparison of L11-α4 sequences, highlighting positions of basic residues. Full alignments are shown in Figure S4A. (B) Diagram of L11-α4-swapped mutants, KHC_{swap} and $Eg5_{Swap}$. (C) Swapping Eg5 L11-α4 into KHC is sufficient to confer end-binding activity. Scale bar: 2 μm. (D) L11-α4 strongly affects microtubule gliding speeds, consistent with it regulating the strong-binding state of the motor. Velocities: KFIC, 606 ± 56 nm/s; $KFIC_{swap}$: 21 ± 2 nm/s; Eg5: 72 ± 2 nm/s; $Eg5_{swap}$: 153 ± 16 nm/s; n_{MT} = 26-37. Mean ± SEM. (E) Number of newly formed microtubule across motor species. 5 μM TMR-labeled microtubules plus 10 vol% DMSO were assembled in the presence or absence of 130 nM motors at 37 °C. Representative images are shown in Figure S4B. (F) Microtubule shrinkage rates following tubulin-washout, showing that L11-α4 confers microtubule stabilization activity. Assays used 80 nM dimeric motors; control and Eg5 groups were taken from Figure 2F (n_{MT} = 13-42). (G) Microtubule growth rates showing that L11-α4 contributes to growth enhancement activity of Eg5. Assays used 20 μM tubulin in the presence or absence of 10 nM dimeric motors; control and Eg5 groups were taken from Figure 2D (n_{MT} = 16-27). See also Figure S4.

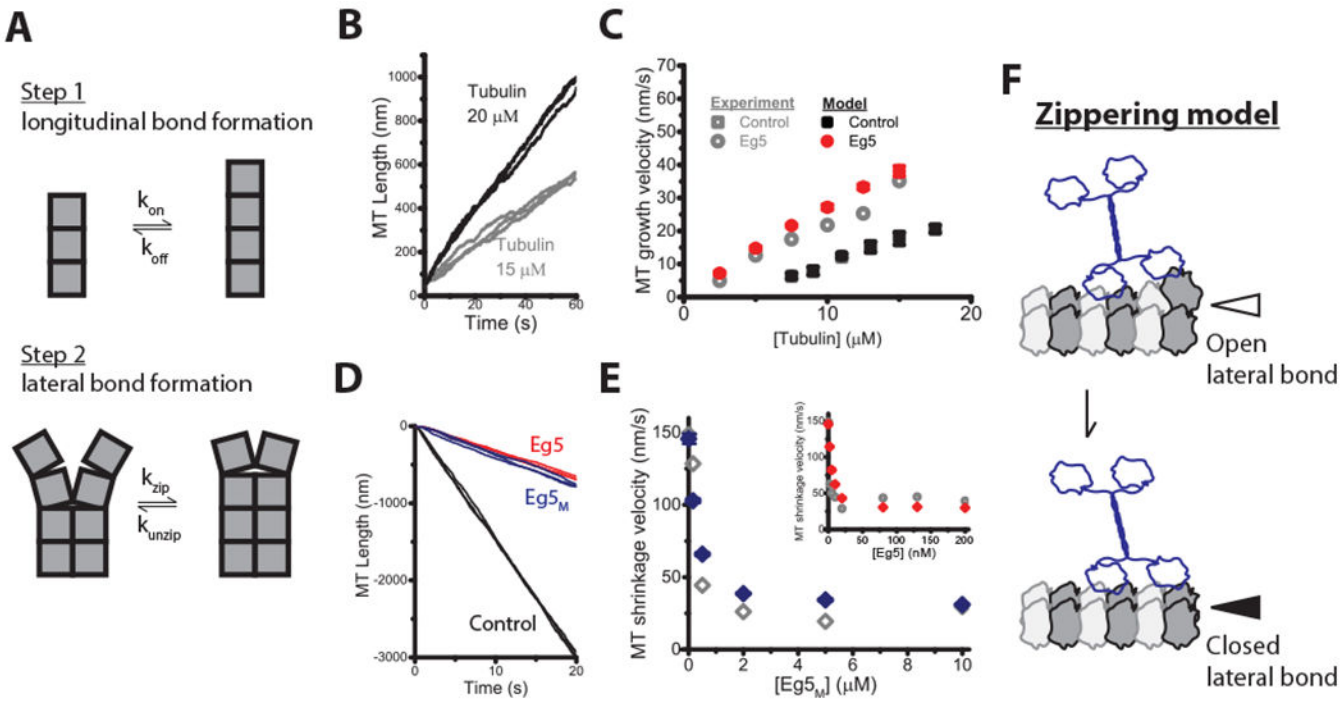

Figure 5. Eg5 polymerase can be explained by Eg5 enhancing tubulin lateral bond energy by 3 k_BT.

(A) Microtubule plus-tip growth is simulated by separating tubulin incorporation into: (Step 1) formation of a single longitudinal bond governed by rate constants k_{on} and k_{off}, followed by (Step 2) formation of a lateral bond with rate constants k_{zip} and k_{unzip}. The sequence is reversed during microtubule shrinkage. (B) Three simulated traces of microtubule growth at 15 μM and 20 μM tubulin in the absence of Eg5. (C) Experimental (from Figure 2E) and simulated microtubule growth velocity across a range of tubulin concentrations. (D) Three simulated traces of microtubule shrinkage in the presence or absence of motors. (E) Experimental (from Figure S2E) and simulated shrinkage rates at varying $Eg5_M$ (main figure) and Eg5 dimer (inset) concentrations. (F) Zippering model of Eg5-induced microtubule polymerization. Plus-end-bound Eg5 motors induce tubulin curved-to-straight transition at tip, thereby promoting lateral bond formation, which enhances the microtubule growth rate and stabilizes microtubules against shrinkage. See also Table S1 for model parameters and Table S2 for tubulin lattice free energy and kinetic parameters.

KEY RESOURCES TABLE

REAGENT or RESOURCE	SOURCE	IDENTIFIER
Antibodies		
His-Tag Antibody	Thermo Fisher	R932-25
Chemicals		
GMPCPP	Jena Biosciences	NU-405L
GTP	Jena Biosciences	NU-1012-LYO
GDP	Jena Biosciences	NU-1172
AMPPNP	Jena Biosciences	NU-214
ATP	Sigma	A2383
ADP	Sigma	A2754
Mant-ADP	Thermo Fisher	M12416
$MgCl_2$	Quality Biological	7058629
DMSO	VWR	WN182
BRD9876	Tocris	5454
Colchicine	Sigma	C9754
Demecolcine	Sigma	D7385
Nocodazole	Sigma	M1404
Maytansinoid DM1	MedChemExpress	HY-19792
Paclitaxel	Sigma	T7191
α-casein	Sigma	C6780
Catalase	Sigma	C1345
Glucose Oxidase	Sigma	G6641
1H,1H,2H,2H-Perfluorodecyltrichlorosilane	Abcam	L16584
β-mercaptoethanol	Sigma	M6250
NeutrAvidin	Thermo Fisher	31000
Methyl cellulose	Sigma	M0512
Bacterial and Virus Strains		
E. coli, DH5α	NEB	C2987I
E. coli, BL21(DE3)	NEB	C2527I
Critical Commercial Assays		
EnzChek	Thermo Fisher	E6646
Q5 Site-directed Mutagenesis kit	NEB	E0554
Recombinant DNA		
Eg5-GFP	[45]	N/A
KHC-GFP	[45]	N/A
Eg5-406	[21]	N/A
KHC-406	[36]	N/A
$Eg5_M$	[22]	N/A

REAGENT or RESOURCE	SOURCE	IDENTIFIER
KHC_M	This study	N/A
$KLP67A_M$	This study	N/A
$Eg5_{swap}$-GFP	This study	N/A
KHC_{swap}-GFP	This study	N/A
$Eg5_{swap}$	This study	N/A
KHC_{swap}	This study	N/A
Software and Algorithms		
MATLAB	Mathworks	https://www.mathworks.com
ImageJ	NIH	https://imagej.nih.gov/ij/
Micro-Manager	Vale Lab	https://micro-manager.org/
MetaVue 6.3	Molecular Devices	https://de.moleculardevices.com/
Clustal Omega	EMBL-EBI	https://www.ebi.ac.uk/Tools/msa/clustalo/
Soft MaxPro 5.4.6	Molecular Devices	https://www.moleculardevices.com/
Pro-Data SX/Viewer	Applied Photophysics	https://www.photophysics.com/
RFPC 5301	Shimadzu Scientific	https://www.ssi.shimadzu.com/support/
OriginLab Pro 9.1	OriginLab	https://www.originlab.com/
UCSF Chimera	UCSF RBVI	https://www.cgl.ucsf.edu/chimera/